

Supplementary materials

Tunable electronic and optical properties of MoTe₂/black phosphorene van der Waals heterostructure: a first-principles study

Qing Chu^a, Bo Peng^{a*}, Lei Yuan^a, Yuming Zhang^a, Renxu Jia^a, Lianbi Li^b

^a *Key Laboratory of Wide Band-Gap Semiconductor Materials and Devices, School of Microelectronics, Xidian University, Xi'an, 710071, China*

^b *School of Science, Xi'an Polytechnic University, Xi'an, 710048, China*

** Corresponding author.*

E-mail address: boopeng@xidian.edu.cn (Bo Peng)

Supplementary Material S1:

As shown in Fig. S1(a), four possible configurations of the heterojunction were considered to obtain the most stable MoTe₂/BP vdWH for subsequent calculations. The variation of binding energy with interlayer spacing exhibits consistent trends across all four configurations as shown in Fig. S1(b). The interlayer spacings and binding energies of the four configurations as shown in Table S1. Therefore, the configuration with the minimum binding energy ($E_b = -0.074$ eV) and smallest interlayer spacing ($d = 3.50$ Å) was selected for subsequent calculations. The electron localization functions (ELFs) for isolated MoTe₂, BP monolayers and MoTe₂/BP vdWH are shown in Fig. S1(c)-(e), which the covalent character for the Mo(P)-Te(P), and no electron is localized in the region between MoTe₂ and BP monolayer for heterostructure, indicating that the vdWHs is composed of weak van der Waals interactions.

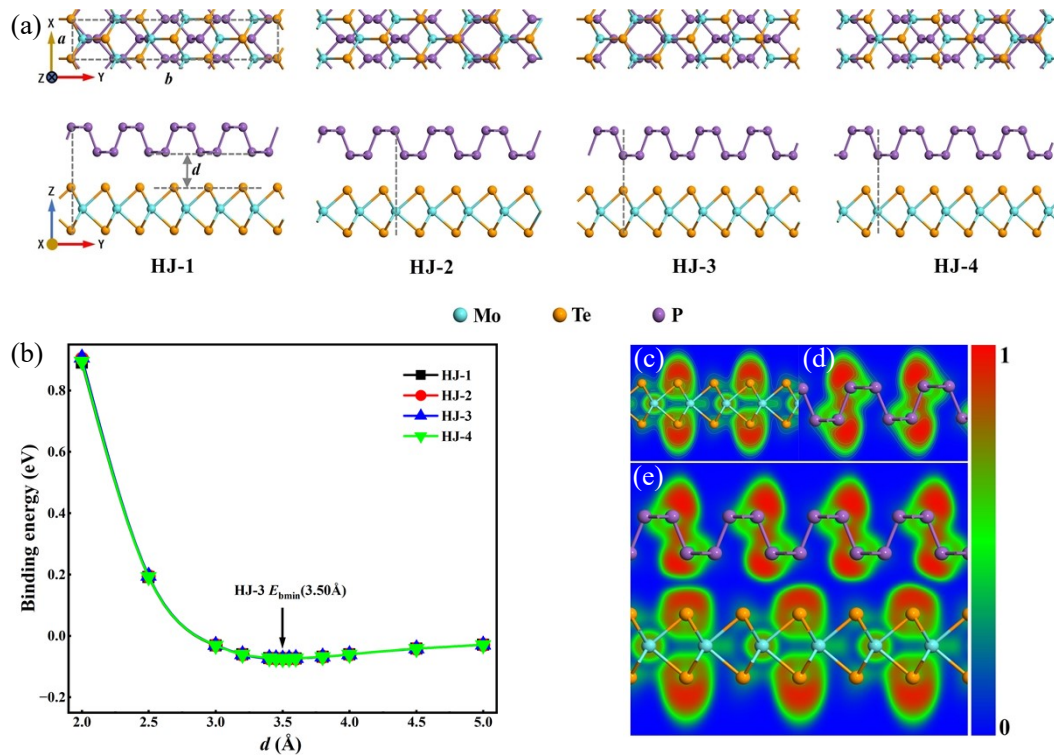


Fig. S1 (a) Four possible configurations of the heterojunction; (b) The binding energy E_b of MoTe₂/BP vdWH under various interlayer spacings; (c) the ELFs of 2H-MoTe₂, (d) BP, and (e) MoTe₂/BP

Table S1 Interlayer spacings of HJ-1, HJ-2, HJ-3, and HJ-4 configurations at minimum binding energies.

	HJ-1	HJ-2	HJ-3	HJ-4
d (Å)	3.52	3.52	3.50	3.51
E_b (eV)	-0.073	-0.073	-0.074	-0.074

Supplementary Material S2:

As shown in Fig. S2, we performed projected band structure analysis on the heterojunction to elucidate the contributions of individual atomic orbitals to the conduction band minimum (CBM) and valence band maximum (VBM). By analyzing the orbital weight distributions at the CBM and VBM, we observed that the P-*p* orbitals, Mo-*d* orbitals, and Te-*p* orbitals all contribute to the CBM and VBM of the heterojunction. Notably, the Mo-*d* orbitals exhibited maximal weight contribution at the CBM, while the Te-*p* orbitals dominated the VBM. It is revealed that the atomic orbitals of MoTe₂ predominantly govern the band edges of the heterojunction, as they contribute most significantly to both the CBM and VBM. Consequently, a straddling band structure emerges, characterized by a type-I band alignment.

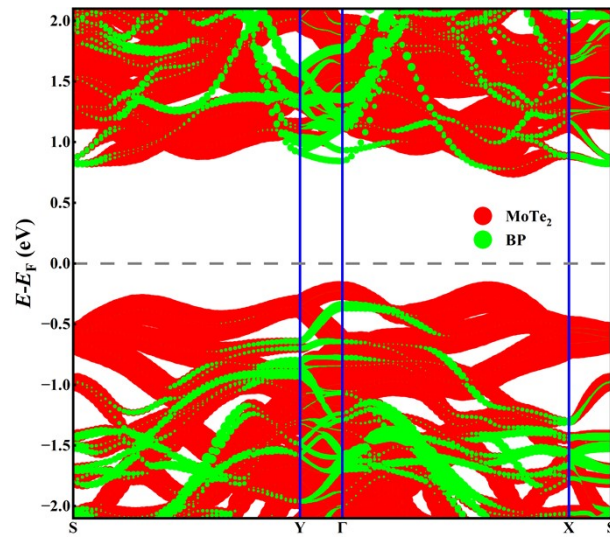


Fig. S2 The projected band structure of the MoTe₂/BP heterojunction.

Supplementary Material S3:

1) Monolayer MoTe₂: As shown in Fig. S3 (a), the significant band splitting was observed at the VBM with SOC, which correlates with the intrinsic topological properties of MoTe₂. Compared to the case without SOC, the bandgap decreased by 0.13 eV while maintaining direct bandgap characteristics in both cases.

2) Black Phosphorene (BP): As shown in Fig. S3 (b), the band structure exhibited minimal sensitivity to SOC, with only a 0.01 eV variation in bandgap and preserved direct bandgap. This indicated that the SOC in black phosphorene is remarkably weak.

3) MoTe₂/BP vdWH: As shown in Fig. S3 (c), the bandgap of the MoTe₂/BP vdWH exhibits only a slight variation of 0.07 eV with SOC and maintained indirect bandgap characteristics.

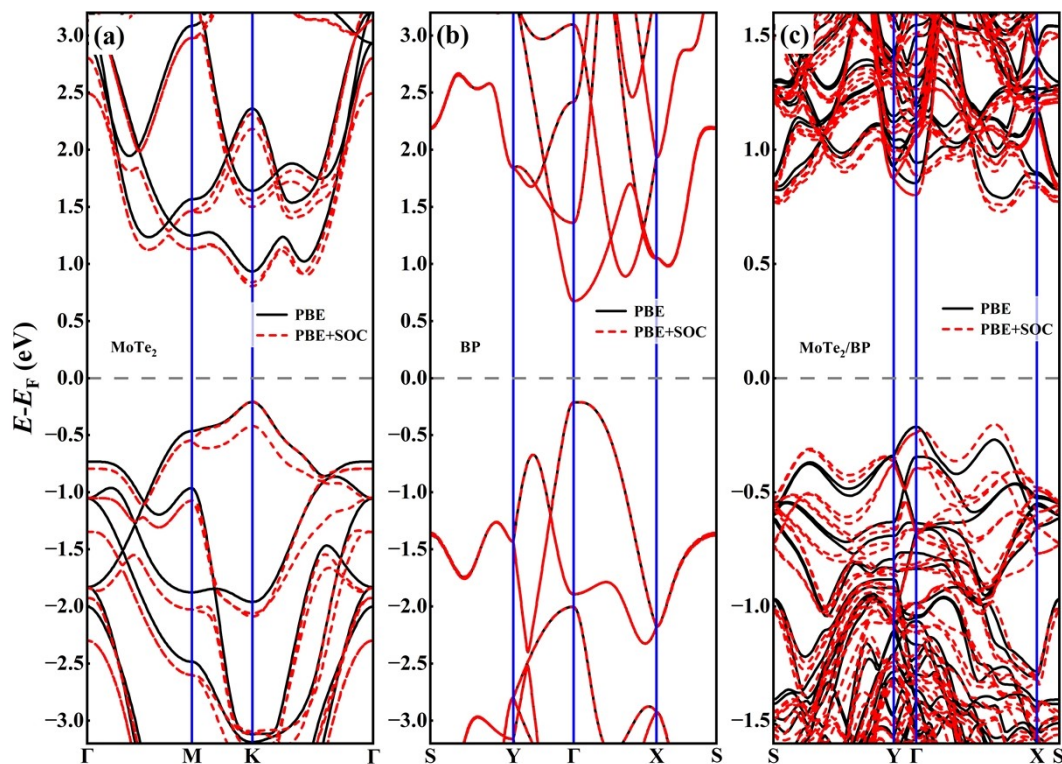


Fig. S3 The band structures of (a) monolayer MoTe₂, (b) black phosphorene (BP), and (c) MoTe₂/BP heterojunction with and without spin-orbit coupling (SOC).

Table S2 The bandgaps of monolayer MoTe₂, black phosphorene (BP), and MoTe₂/BP heterojunction.

	HSE06 (eV)	PBE (eV)	PBE+SOC (eV)	σE_g (eV)	i/d
MoTe ₂	1.6	1.14	1.01	0.13	d
BP	1.59	0.89	0.88	0.01	d
MoTe ₂ /BP	1.44	1.01	0.94	0.07	i

σE_g represents the difference in band gap between PBE and PBE+SOC; i/d represents indirect bandgap and direct bandgap, respectively.

Supplementary Material S4:

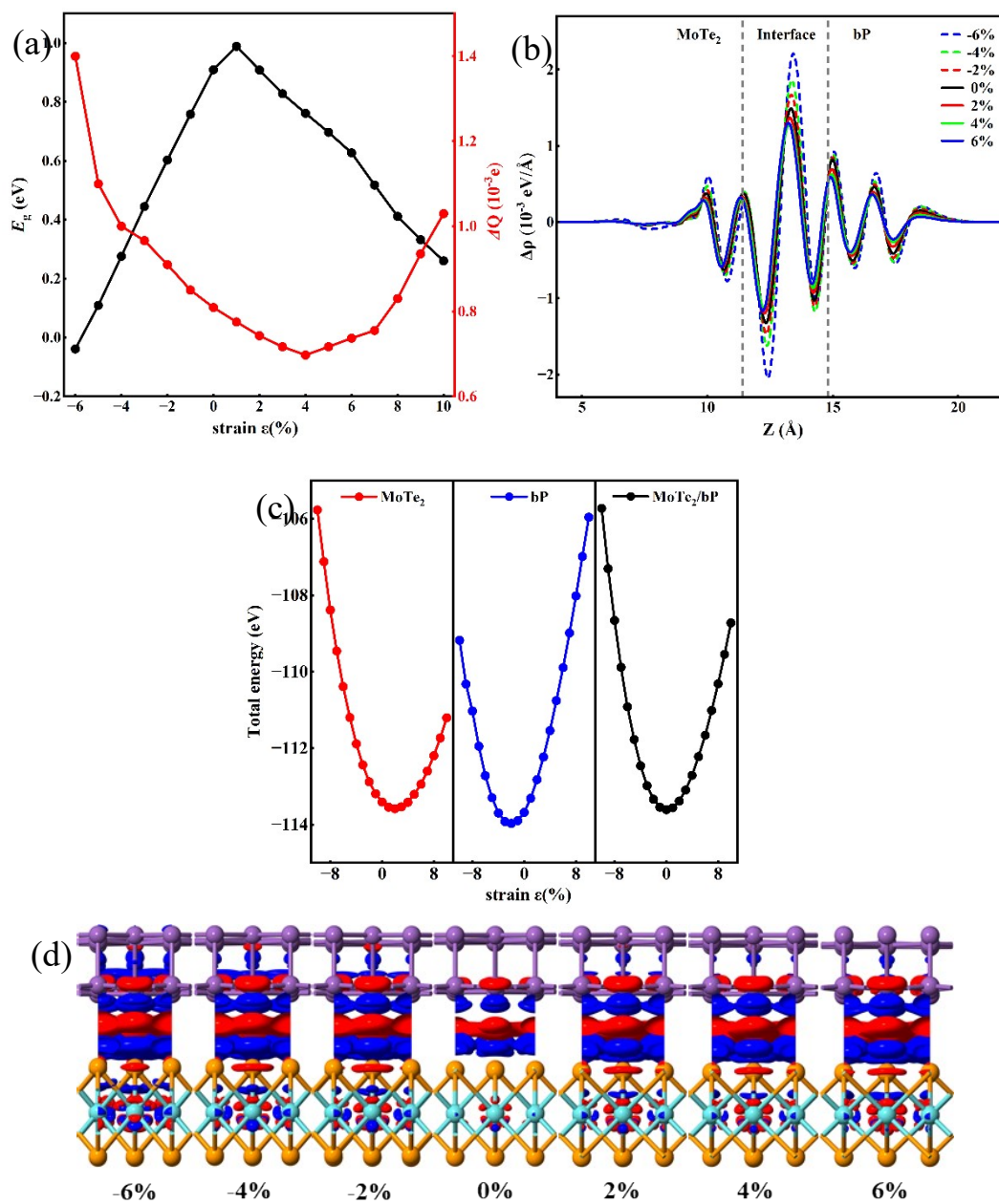


Fig. S4 (a) The bandgap and ΔQ of MoTe₂/BP vdWH under various biaxial strain. (b) The plane-averaged CDD and (d) 3D isosurface (with the isovalue of $0.002 \text{ e}/\text{\AA}^3$). (c) The total energy of MoTe₂, BP and MoTe₂/BP vdWH under various biaxial strain.

Supplementary Material S5:

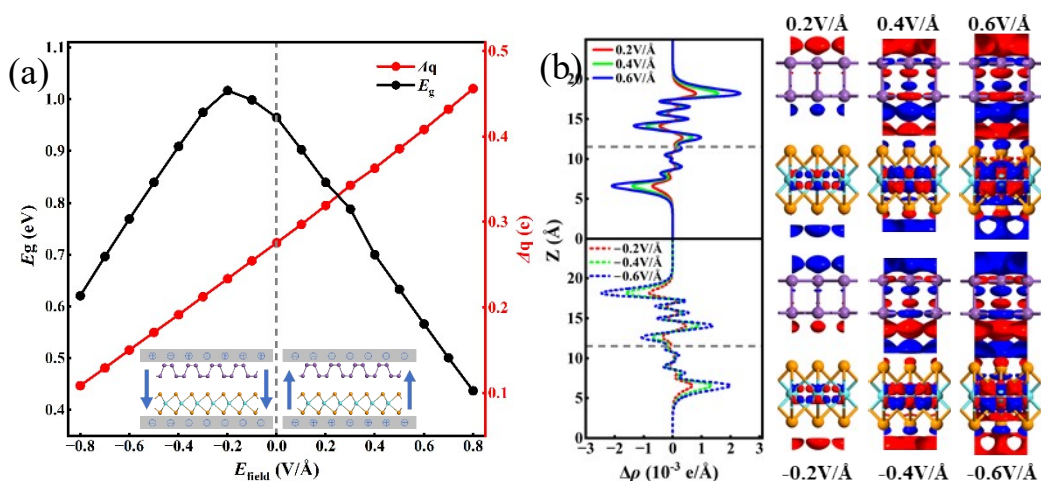


Fig. S5 (a) The bandgap E_g and Bader charge of MoTe₂/BP vdWH under various electric field. (b) The plane-averaged CDD and 3D isosurface (with the isovalue of 0.001 e/Å³),

Supplementary Material S6:

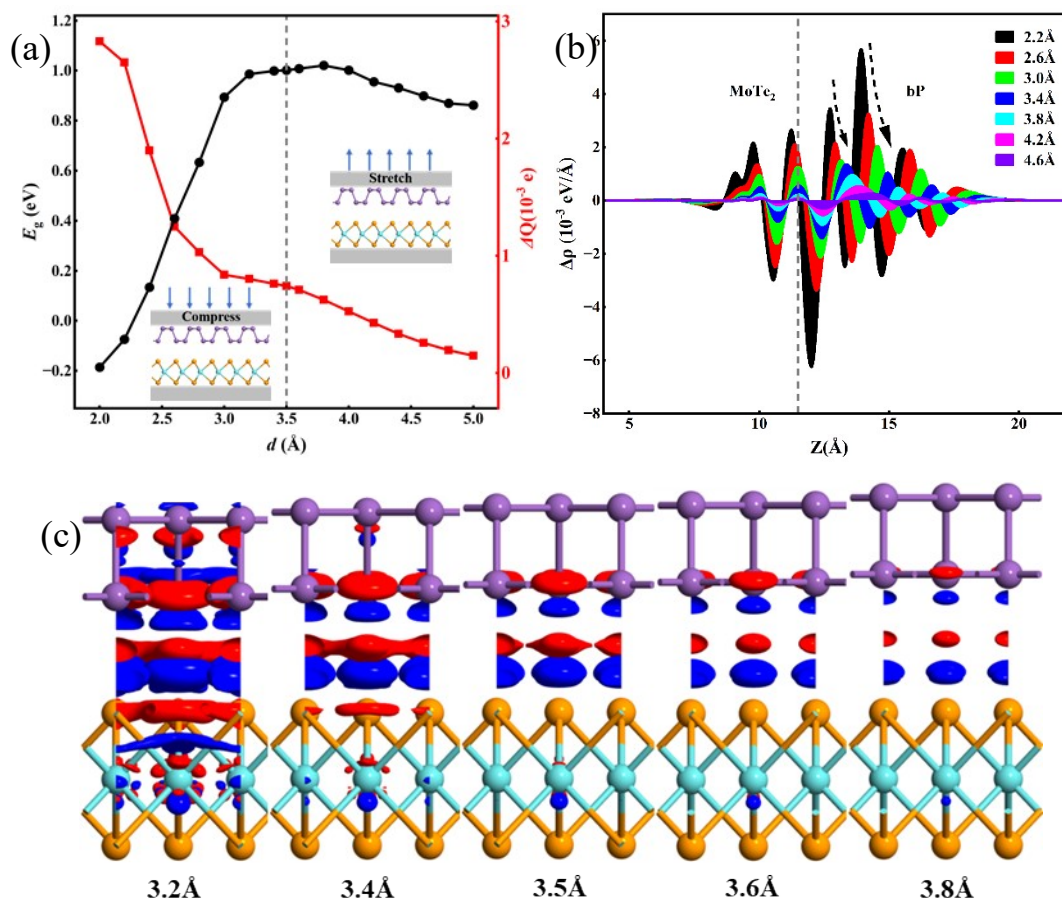


Fig. S6 (a) The bandgap E_g and ΔQ of MoTe₂/BP vdWH under various interlayer spacings. (b) The plane-averaged CDD and (c) 3D isosurface (with the isovalue of 0.0035 e/Å³)

Supplementary Material S7:

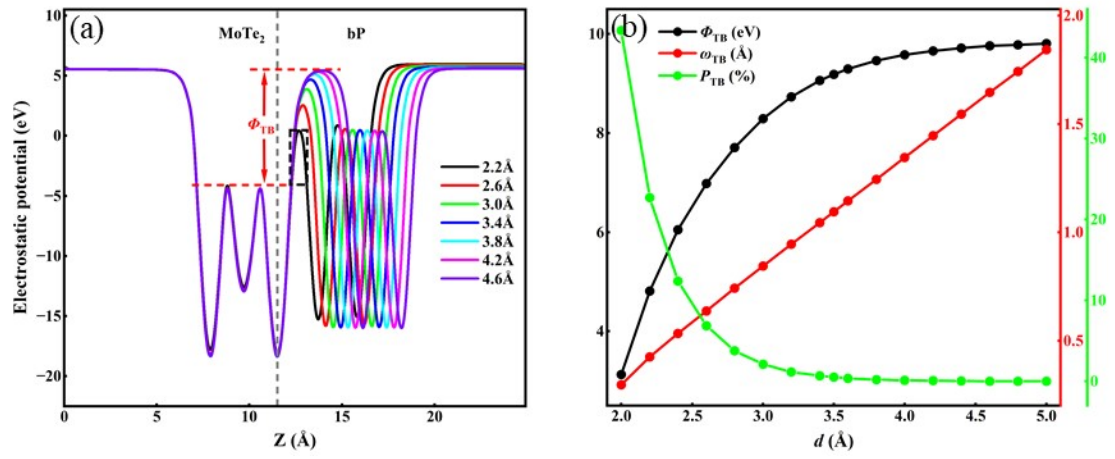


Fig. S7 (a) The electrostatic potentials and (b) tunneling probability (P_{TB}), tunneling barrier height (Φ_{TB}) and width (ω_{TB}) of MoTe₂/BP vdWH under various interlayer spacings, respectively.